

Lateral growth of MoS₂ 2D material semiconductors over an insulator via electrodeposition

Nema M. Abdelazim^{1,*}, Yasir J. Noori^{1,*†}, Shabin Thomas^{2,*}, Victoria K. Greenacre², Yisong Han³, Danielle E. Smith², Giacomo Piana¹, Nikolay Zhelev², Andrew L. Hector², Richard Beanland³, Gillian Reid², Philip N. Bartlett², C. H. (Kees) de Groot^{1,†}

¹School of Electronics and Computer Science, University of Southampton, Southampton, SO17 1BJ, UK

²School of Chemistry, University of Southampton, Southampton, SO17 1BJ, UK

³Department of Physics, University of Warwick, Coventry, CV4 7AL, UK

*These authors contributed equally to this work.

† y.j.noori@soton.ac.uk; chdg@ecs.soton.ac.uk

Abstract

Developing novel techniques for depositing transition metal dichalcogenides is crucial for the industrial adoption of 2D materials in optoelectronics. In this work, we have demonstrated lateral growth of molybdenum disulfide (MoS₂) over an insulating surface using electrochemical deposition. By fabricating a novel electrode structure, we can connect electrodeposited MoS₂ grown from TiN electrodes on opposite sides across an insulating substrate, thus forming a lateral device structure using just one lithography and deposition step. Using a variety of characterisation techniques, we have shown that the lateral growth rate of MoS₂ is over 20 times higher than its vertical growth rate. We performed electronic and photo-response measurements on the device structures and confirmed that our material behaves like semiconducting MoS₂, confirming its potential for photodetection applications. This result paves the way towards developing the lateral growth electrodeposition technique for other transition metal dichalcogenide 2D materials as well as their lateral heterostructures.

Keywords: Electrodeposition, non-aqueous, transition metal dichalcogenides, molybdenum disulfide, lateral growth, titanium nitride, photodetector

1. Introduction

Molybdenum disulfide is a two-dimensional (2D) transition metal dichalcogenide (TMDC) material that has been used as building blocks in demonstrations of high on/off ratio transistors, ultrasensitive photodetectors and sensors.^{1–4} Some of these demonstrations were implemented for wearable applications by exploiting the material's exceptional robustness and flexibility.^{5,6} However, there remain major obstacles that hinder the industrial adoption of MoS₂ and other 2D TMDC materials. The most challenging obstacle has been finding an industrially compatible method that enables the production of these materials on a mass scale. We have recently demonstrated that electrodeposition is a potentially viable method for solving this challenge to create large-area and continuous 2D films.^{7,8} Electrodeposition offers important advantages in 2D material production over other methods such as chemical vapour deposition (CVD),^{9,10} sputtering¹¹ or atomic layer deposition (ALD).¹² Electrodeposition is not a line-of-sight deposition method as material growth occurs at electrical contacts and is controlled by electrical potential or current.¹³ It can hence be utilised to deposit materials over three dimensional surfaces including patterned nanostructures of high aspect ratios.^{14–17} In addition, electrodeposition is not performed in harsh environments that involve plasma or extremely high temperatures which can damage pre-existing materials on the substrate, such as graphene electrodes.⁷

However, there are critical limitations with electrodeposition that need to be overcome. Firstly, the crystallinity of electrodeposited MoS₂ films is not as high as ones deposited via CVD.¹⁸ Secondly, electrodeposition requires an electrically conductive surface from which materials are traditionally grown vertically upwards.¹⁹ Depositing a semiconductor material on a conductor provides a low resistance current path in planar (opto-) electronic devices such as transistors, thus limiting the use of

electrodeposition traditionally to certain vertical device structures or metal interconnects (through the dual damascene process).²⁰ This limitation is a drawback specifically for developing 2D material based devices where planar structures that exploit the unique 2D properties of the material are the “natural” route forward.^{21–24}

Creating innovative techniques to electrodeposit planar 2D materials over non-conducting surfaces would solve this limitation and open new routes where the insulator base can be utilised, such as in transistor gating. In the early 2000s, attempts were made to electrodeposit materials over insulating substrates and conductive polymers.^{25–29} Metal films and nanowires were grown laterally using electrodeposition from conductive electrodes over graphite and dielectrics. Kobayashi *et al.* went one step further and showed that significant enhancement in the lateral growth rate of Au can be achieved via the surface treatment of SiO₂.³⁰ However, in all of these works the deposits were elemental metals, thus limiting the scope of applications for which this technique can be employed.

In this work, we demonstrate the lateral growth of thin MoS₂ semiconductor films by electrodeposition over insulating substrates. By fabricating micro-electrodes with a top insulator, leaving only the thin edges of the electrode exposed, we were able to restrict the initial nucleation and growth of the MoS₂ films to these thin edges. Based on the anisotropic structures of layered TMDCs, we can exploit the faster rate of in plane growth compared to out of plane growth. Using various material characterisation techniques, we show that the lateral growth rate of MoS₂ across the insulator is more than an order of magnitude larger than its vertical growth. Furthermore, we have shown that we can controllably connect MoS₂ films grown from the thin electrodes on either side of the insulating surface to make a device structure via a single lithography step. We then demonstrate that our laterally grown MoS₂ films are

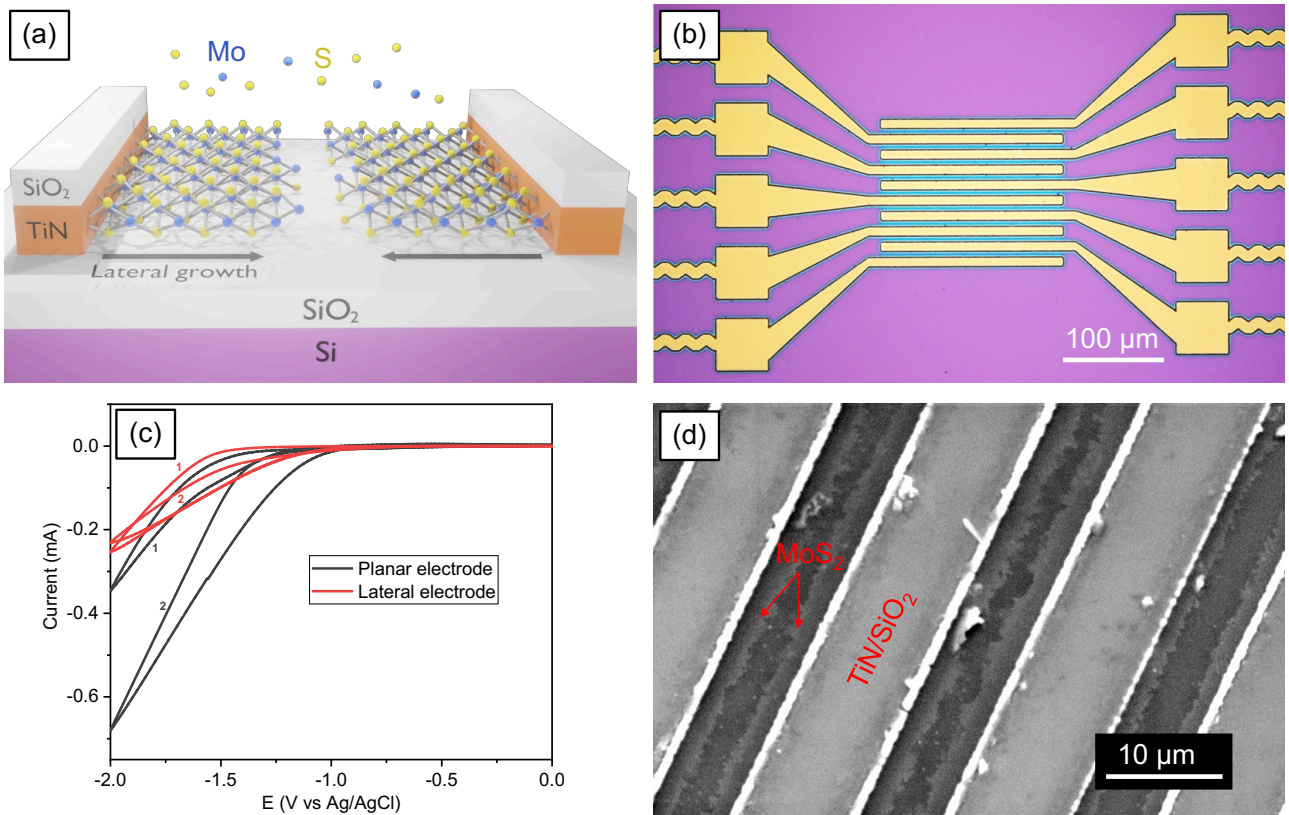


Fig. 1 (a) An illustration of the concept of this work showing TiN electrodes that are top covered with a SiO₂ insulator with a TMDC MoS₂ film growing laterally on the SiO₂/Si substrate. (b) A microscope image of the fabricated electrode structure showing 10 adjacent electrodes each connected to a pad for electrical contact. The light blue colour surrounding the edges of the electrodes is laterally grown MoS₂ (c) Cyclic voltammetry electrodeposition scans comparison between a large-area planar TiN electrode (diameter 4 mm) and one of the TiN lateral growth electrodes. (d) An SEM image showing four TiN electrodes and three micro-gaps that are partially filled with laterally grown MoS₂ films via electrodeposition.

semiconductors by electrical measurements and photoresponsivity.

2. Experimental Section

Lateral growth electrodes fabrication

An illustration of the concept of our work on the lateral electrodeposition of MoS₂ is shown in Fig. 1 (a). The TiN electrodes were fabricated on a SiO₂/Si substrate using a single photolithographic step as shown in Fig. S1. First a negative photoresist was spin-coated on a wafer and then UV exposed using a photolithographic mask to form the desired pattern. TiN and SiO₂ were then consecutively sputtered on the wafer before both materials were lift-off to form the lateral growth electrodes. The thickness of the sputtered TiN layer is approximately 100 nm. The double layer lift-off was executed to minimise the number of fabrication steps, and to eliminate the possibility of mis-alignment between the two sputtered layers that could result from performing multiple lithographic steps. A microscope image of the electrodes is shown in Fig. 1 (b). The wafer was then diced into smaller chips prior to the MoS₂ electrodeposition. An illustration of the chip layout is shown in supplementary Fig. S2. After MoS₂ deposition, each chip is cleaved into two halves through the cutting zone shown to disconnect the global electrode and to create individual devices.

Electrodeposition of MoS₂

The electrodeposition experiments were performed in CH₂Cl₂ solvent using [NⁿBu₄]₂[MoS₄], which was synthesised in-house to function as a single source precursor, providing both the Mo

and S.^{7,8} In contrast to [NH₄]₂[MoS₄], which is more commonly used in aqueous solvents, [NⁿBu₄]₂[MoS₄] has excellent solubility in CH₂Cl₂. The electrodeposition solution also included [NⁿBu₄]Cl as the supporting electrolyte and trimethylammonium chloride [NHMe₃]Cl as the proton source, which is necessary to remove the excess S during deposition of MoS₂ from MoS₄²⁻.⁸ The electrodeposition experiments were all performed within a glovebox equipped with a nitrogen circulation system to minimise moisture and ensure that oxygen levels are maintained below 10 ppm. The depositions were performed using a three electrode electrochemical cell with a Pt gauze as counter electrode and a Ag/AgCl (0.1 M [NⁿBu₄]Cl in CH₂Cl₂) reference electrode.

Cyclic voltammetry (CV) scans were performed to study the electrochemical behaviour of the electrolyte with the lateral growth electrodes. Fig. 1 (c) shows the comparison of CVs recorded on a TiN fabricated electrode and a 4 mm diameter planar TiN electrode. The CV is obtained by sweeping the voltage from 0 to -2.0 V in the cathodic scan and then -2.0 to 0 V in the anodic scan. The arrows in the figure indicate the directions of the sweep. On the first cycle there is evidence of a nucleation process in both cases with the current being increased on the return and on subsequent scans. This occurs because the deposited MoS₂ catalyses the reduction of the NHMe₃⁺ and the evolution of hydrogen. We recently reported a detailed investigation on the electrochemical processes during the CV of the same electrolyte system employing an electrochemical quartz crystal microbalance (EQCM) measurements.⁸ The CVs displayed in Fig. 1 (c) clearly shows evidence of the cathodic reduction of [MoS₄]²⁻ ions to MoS₂. It is clear that the CV

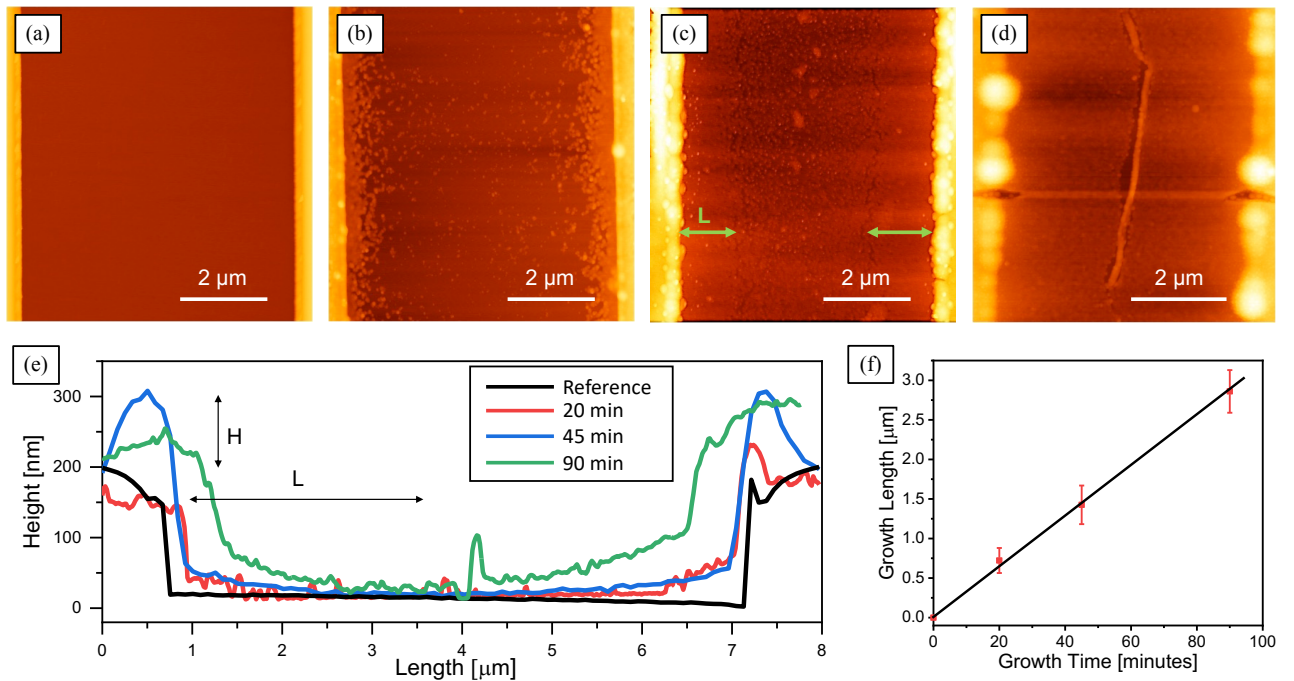
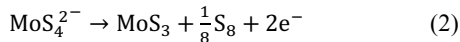
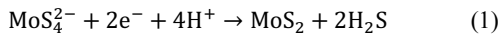


Fig. 2 AFM images of (a) reference sample and (b-d) laterally grown films deposited for (b) 20 min, (c) 45 min and (d) 90 min after anneal. (e) Topography line profiles collected from images (a-d). The figure shows indications of the vertical growth (H) and lateral growth (L) that were considered for analysis in this work. (f) A linear fit of the growth length vs time obtained from the three samples.

recorded from the lateral TiN electrodes is comparable, in terms of electrochemical processes at the interface, to the CV measured on the planar TiN electrode, indicating that the electro-reduction mechanism of the [MoS₄]²⁻ ions remains the same irrespective of the type of TiN electrode used.

The lateral growth of MoS₂ was achieved through potentiostatic electrodeposition by applying -1.0 V and varying the deposition time to achieve the desired lateral growth length. The electrochemical reactions at the working and counter electrodes respectively, are as follows



Following electrodeposition, the sample was rinsed with CH₂Cl₂ and left to dry inside the glove box. The as-deposited MoS₂ film is amorphous as X-ray diffraction on thicker films indicate, although with some short-range ordering present as evidenced by the preferential lateral growth.^{8,31-33} An annealing step was performed to crystallise the film. The sample was annealed using a tube furnace that was set initially to 100 °C for 10 min and then 500 °C for 2 h at 0.1 mbar. Annealing the films was performed within a sulfur rich environment made by placing 0.1 g of sulfur powder together with the sample inside the quartz tube within the tube furnace.

3. Results and Discussions

Microscopy

On applying an electrodeposition potential to the electrode array, the material starts to grow from the side edges of each electrode. Fig. 1 (b) shows an optical microscope image of patterned electrodes with laterally grown MoS₂ films depicted by the light blue borders surrounding the yellow electrodes. Fig. 1 (d) shows a scanning electron microscope (SEM) image of the MoS₂ grown

laterally from the edges of the TiN electrodes. The contrast difference between the laterally grown MoS₂ films and the SiO₂ covered substrate underneath can be clearly observed. The film in this figure was grown by electrodeposition for 45 minutes. By observing the electrodeposition rate vs. time, we were able to allow the laterally grown films from adjacent electrodes to contact in the middle region by electrodepositing for 90 minutes. Supplementary Fig. S3 (a-c) shows SEM images of laterally grown films deposited for 20, 45 and 90 minutes.

Fig. 2 (a-d) shows atomic force microscopy (AFM) images performed across the growth regions between two adjacent electrodes from a pristine substrate and ones with laterally grown MoS₂ films. Typical line profiles for each film are shown in Fig 2 (e). The images were acquired for an active area of 7 μm × 7 μm. As observed from the AFM images, the films have grown laterally from both sides of the electrodes. Upon increasing the deposition time to 45 min, the film near to the electrodes were found to be smoother and continuous. However, it is clear from Fig. 2 (c) that 45 min is not sufficient to allow the films grown from opposite sides to contact each other. Fig. 2 (d) shows an AFM image of a film grown for 90 minutes. In the latter deposition, the two films were found to meet in the centre of the SiO₂ substrate, causing one film to grow over the other, resulting in a small peak in the AFM profile in the middle region. Fig. 2 (f) shows that the lateral growth length scales linearly with the deposition time. An average growth rate of 33 ± 6 nm/min was extracted. The error bars represent the maximum and minimum observed growth lengths. The lateral growth length measurements were recorded on the films that were grown out of the upper most electrode from the ten-electrode array shown in Fig. 1 (b). This was chosen to prevent connecting layers from introducing uncertainties in the length measurements. Each experiment with a particular deposition time was replicated to ensure experimental reproducibility. The average lengths and

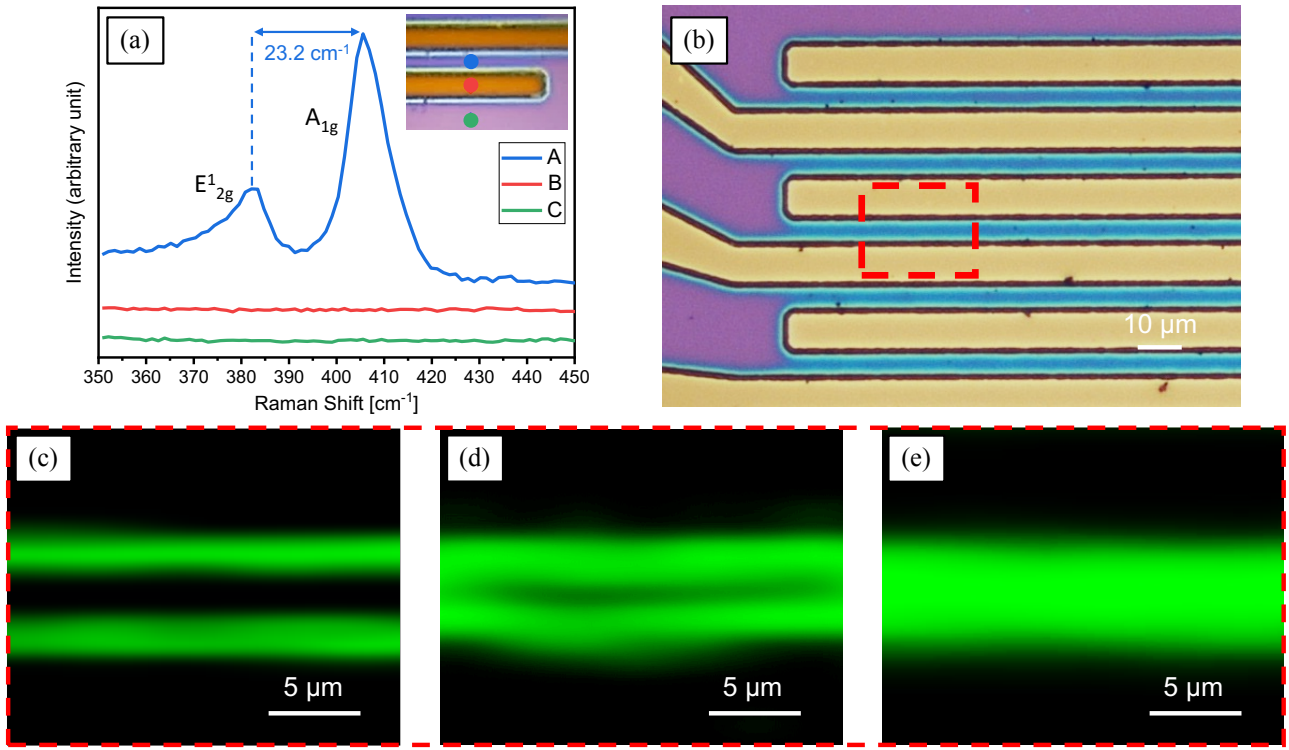


Fig. 3 (a) A stack of Raman spectra showing that the MoS₂ signal is solely observed from the laterally grown films with no Raman signatures from areas away from the electrodes or at the centre above them. (b) An optical microscope image of a series of fabricated TiN micro-electrodes with laterally grown MoS₂ films (90 minutes) that are showing as light blue borders surrounding the electrodes. (c-e) Raman maps of areas corresponding to that of the red box in (b) between adjacent electrodes for films grown for 20, 45 and 90 minutes, respectively. The maps show a clear increase in the lateral length of the MoS₂ films with increasing the deposition time.

uncertainties were calculated over ten AFM measurements from every sample.

reproducibility. The error bars represent the maximum and minimum observed growth lengths. The lateral growth length measurements were recorded on the films that were grown out of the upper most electrode from the ten-electrode array shown in Fig. 1 (b). The average length and uncertainty were calculated over ten AFM measurements from every sample.

As the electrodeposition time is increased, the vertical growth of the material becomes more prominent, especially near the electrodes where the film growth starts. We observed that the vertically grown materials can be thick enough to rise above the fabricated TiN/SiO₂ electrodes and start to grow laterally over the top insulated electrodes. However, it is clear that the vertical growth rate of MoS₂ is much slower than the lateral growth rate. To characterise the vertical growth of MoS₂, topography profiles were acquired from five lines across AFM images corresponding to films grown for 20, 45 and 90 min as shown in supplementary Fig. S4 (a). The average values of the vertical (height) and lateral growths (length) were extracted for each film. The average heights above the edge of the electrodes (H_{av}), lengths (L_{av}) and their corresponding maximum (H_{max} and L_{max}) values were recorded in Table 1 in the supplementary information. Fig. S4 (b) shows the L_{av} and H_{av} measurements taken from five different lines across the 20, 45 and 90 minutes grown films. By comparing the values of H versus W , we found that the lateral growth rate is approximately 20 times larger than the vertical growth.

Raman Spectroscopy

Raman spectroscopy is a commonly used technique in characterising different physical properties of TMDC 2D materials. We used this method to confirm the presence of the MoS₂ films and qualitatively study their degree of crystallinity

and lateral growth length. All measurements were performed using a 532 nm excitation laser at room temperature. A 50x objective lens was used to focus the excitation laser to a ~ 1 μm spot diameter and simultaneously collect the emitted light. Fig. 3 (a) shows three Raman spectra collected from different locations around the electrodes using a sample with a MoS₂ film grown for 45 minutes. Point A is in the centre between the two electrodes, point B is above one of the electrodes, point C is on a blank SiO₂/Si region of the substrate, away from the electrodes. These locations are shown in the inset of the figure. The MoS₂ Raman signature corresponding to the E¹_{2g} and the A_{1g} peaks was only found at point A, demonstrating that there is no deposition at the centre above the top insulated TiN electrodes nor on the SiO₂ substrate away from the electrodes. The central positions of the E¹_{2g} and A_{1g} peaks are 382.5 cm⁻¹ and 405.6 cm⁻¹, respectively. Energy dispersive X-ray (EDX) spectroscopy spectra are shown in Fig. S5. Due to the large overlap between the Mo and S electron emission lines (~ 2.3 keV), EDX is not a reliable technique to measure the elemental composition. It was therefore only used to identify the nature of the materials at different regions of the sample, utilizing the much higher image resolution offered by the SEM compared to optical techniques. The EDX spectra show Mo and S signatures solely above the laterally grown films, confirming the conclusion of the Raman images.

Raman mappings were performed on selected areas as exemplified in Fig. 3 (b) of 20, 45 and 90 minutes grown films using the A_{1g} peak signal intensity and a step size of ~ 1 μm, see Fig. 3 (c-e). The maps show the evolution of the lateral growth as the electrodeposition time is increased, causing the films grown from opposite sides to slowly merge after approximately 90 min deposition. However, the fact that the laser spot is ~ 1 μm means that the exact distribution of the material cannot be precisely defined through this method. The combined results of AFM, SEM, and Raman mapping clearly confirm the lateral

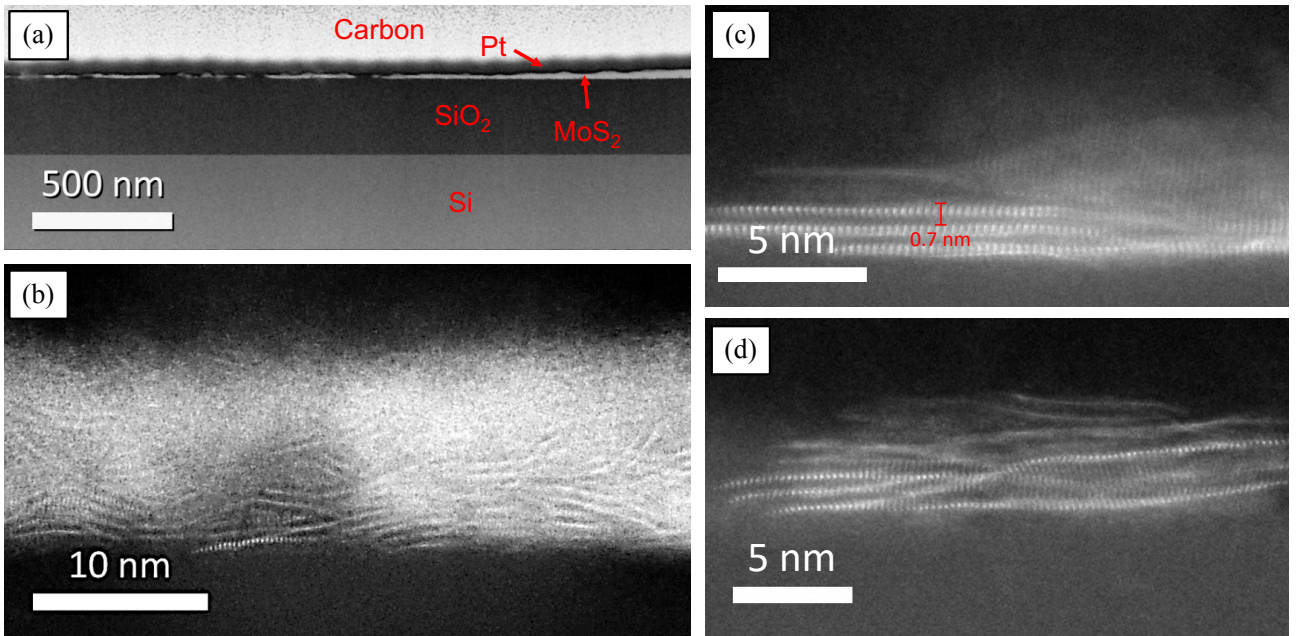


Fig. 4 (a) A high-resolution SEM image of a cross section of a region between two electrodes with a laterally grown MoS₂ film. The film was coated with Pt and C protective layers (b) A magnification of the MoS₂ film shown in (a) taken via TEM that clearly shows the layered nature of the film growing preferentially in the horizontal direction along the surface of the wafer. The film was taken from a sample that was grown for 90 minutes. (c and d) TEM images of a few layers of MoS₂ taken at a thin region from a film that was grown for 45 minutes.

growth of MoS₂ across the SiO₂ insulator after starting from the thin edges of the TiN electrodes.

Transmission Electron Microscopy

Fig. 4 (a) shows a high-resolution SEM image of a cross section of a laterally grown film. The cross-section was taken after performing a lamella process using a focused ion beam (FIB). The image shows the MoS₂ thin film grown over the SiO₂/Si substrate and covered by Pt and C protection layers that were deposited during the lamella process. It can be seen that the film gets thinner further away from the electrode towards the left of the image. Annular dark field (ADF) TEM imaging was then used to reveal the nanocrystalline structure of MoS₂ layers. The ADF mode allows distinguishing MoS₂ from its surrounding SiO₂ and Pt. Fig. 4 (b) shows a laterally grown film which was deposited for 90 minutes. We noticed that the stacked layers are generally aligned in the lateral growth direction perpendicular to the plane of the substrate. In a film grown for 45 minutes, presented in Fig. 4 (c and d), TEM imaging reveals that the film is much thinner and where the layers are more ordered. This suggest that the amount of ordering correlates inversely with the thickness of the films. The layer-to-layer distance of the ordered stack shown in Fig. 4 (c) was measured to be 0.7 ± 0.1 nm, which is in agreement with literature values of MoS₂ layers spacing measurements.³⁴

Photoresponsivity of laterally grown MoS₂ devices

Electrical characterisation of the laterally grown films was performed by connecting adjacent lateral growth electrodes to a semiconductor device analyser. Fig. 6 (a) shows current-voltage sweeps taken from films that were grown for 20, 45, and 90 minutes. The displayed curves were taken from different films that were grown in multiple repeat experiments. The electrical connection between the electrodes for the 20 min sample is open, while that for the 45 minutes sample, has resistance exceeding 500 M Ω . The electrical resistance was measured to be significantly lower for the 90 minutes sample after the laterally grown films from both sides have connected in the middle. The

inset of the figure shows ohmic behaviour with a resistance of ~ 1 M Ω . Using the length and width of the channel and the estimated average thickness of the films (~ 60 nm), we extract the room temperature resistivity of the 90 minutes grown films as $115 \Omega \cdot \text{cm}$. This resistivity is in the range of earlier reported MoS₂ films.³⁵

The photoresponsivity of the MoS₂ films was tested at room temperature in air, using a 532 nm laser source. The aim of this experiment was to test the film's semiconductor optical absorption and induced current. The tests were performed by applying a bias voltage on two adjacent electrodes and the current was measured through the device in the dark and under laser illumination. The laser light was coupled to the chip through a fibre and a long distance 20x objective lens, reducing the spot size to a circular spot with a diameter of roughly 100 μm . Fig. 6 (b) presents the photocurrent induced in the material due to a pulsing laser. The applied bias, $V_{\text{bias}} = 1$ V and the laser power density was calculated to be around $6 \times 10^4 \text{ W m}^{-2}$. The photoresponsivity of the film was calculated using equation (3) below:

$$\text{Photoresponsivity} = \frac{I_{\text{ph}}}{P_{\text{laser}}} \quad (3)$$

where I_{ph} is the photoinduced current. I_{ph} can be calculated by subtracting the device current under illumination from the dark current ($I_{\text{ph}} = I_{\text{light}} - I_{\text{dark}}$) and P_{laser} is the incident laser power. Several measurements were made on different chips containing devices of films grown for 90 minutes. The maximum photoresponsivity recorded was 0.9 mA W^{-1} . We then performed photoresponsivity measurements at varying laser power density as shown in Fig. 6 (c).

It was found that the photoresponsivity reduces at higher laser power density, indicating carrier saturation in the material. Whilst this photoresponsivity is higher than our previously values reported from the electrodeposition method,⁷ it is still lower than previously reported from MoS₂ films made via CVD and mechanical exfoliation^{36,37}. This is expected to be due to the

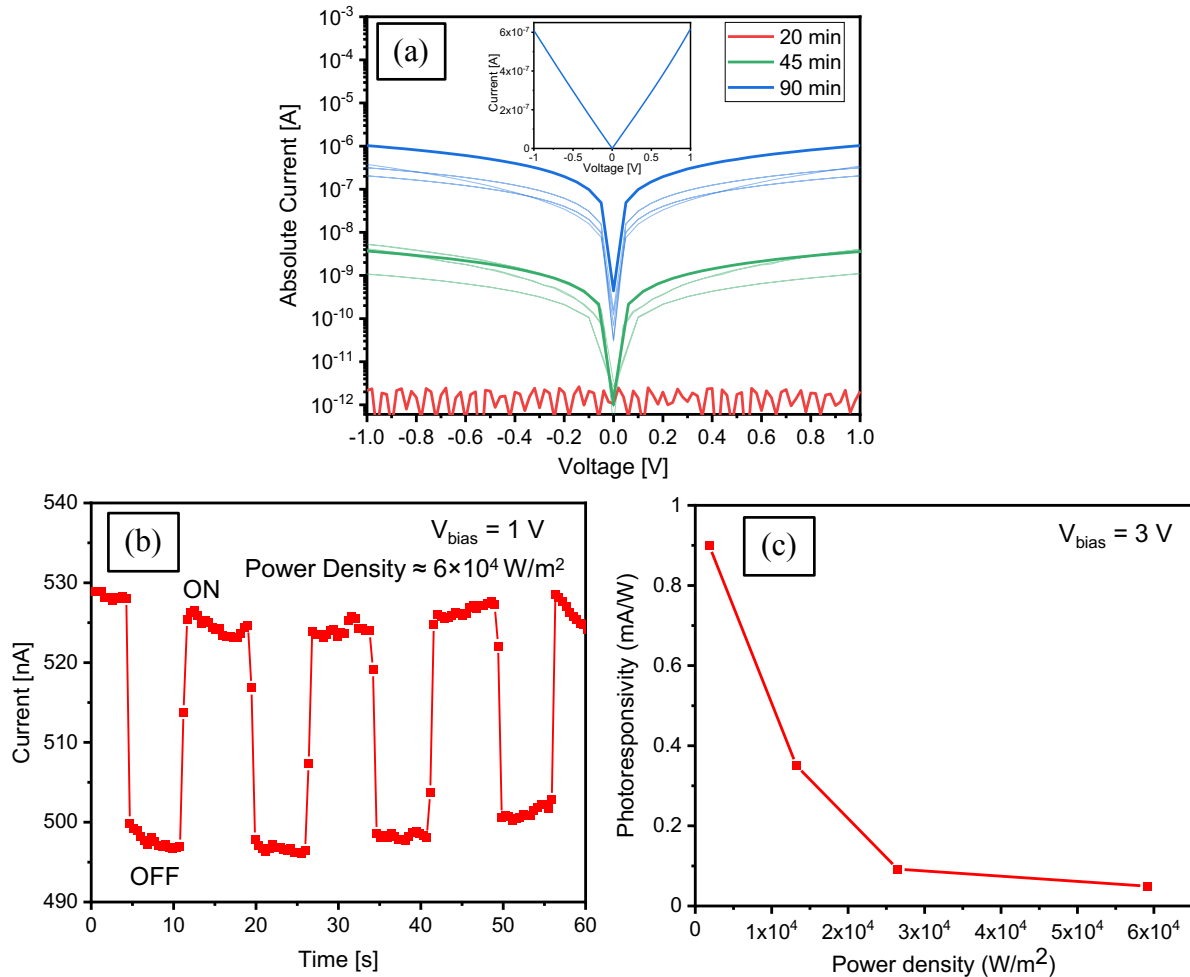


Fig. 5 (a) Multiple Current-Voltage sweeps from MoS₂ devices grown multiple times for 20, 45 and 90 minutes showing an open circuit after 20 min film growth and a great increase in current from 45 min growth to 90 minutes. (b) photo-illumination cycles of a sample showing the switching induced photocurrent with a switching laser source. (c) The change in photoresponsivity as the power density of the excitation laser is changed.

lower material crystallinity produced from electrodeposition in comparison to the other aforementioned methods. Our future work will include using a similar structure to develop phototransistor devices using the bottom SiO₂ as a back-gate dielectric.^{2,9}

4. Conclusions and Outlook

We have demonstrated the lateral electrodeposition of transition metal dichalcogenide (TMDC) films over an insulating substrate for optical and electrical measurements. The MoS₂ is deposited directly onto patterned electrodes using a non-aqueous electrodeposition method. The nature of the deposition is such that the material growth occurs from the side edges of 100 nm thick TiN electrodes. The electrodeposition duration determines the extent of the material's lateral growth. By fabricating adjacent electrodes and exploiting the preference of the material to grow laterally, we have shown the ability to grow films from opposite sides towards each other until they connect in the middle. The deposited films were characterised using a variety of techniques including AFM, Raman, SEM, EDX, and TEM. The lateral growth length was found to increase linearly with the deposition time with an average rate of $\sim 33 \pm 6$ nm/min. This is over an order of magnitude faster than the material's vertical growth. Electrical and photoresponsivity measurements of the MoS₂ films showed that the material is semiconducting. Our

work provides an innovative, efficient and scalable method for the lateral growth of 2D materials and promotes their applications in next-generation electronic and optoelectronic devices. This paves the way towards future possibilities such as electrodepositing different TMDCs to form lateral heterostructures of 2D materials, creating novel p-n-p junction in a single electrodeposition experiment.^{38,39}

Author Contributions

NA, YJN, GP and CHDG fabricated the electrodes and characterised the electrodeposited materials, ST, NZ and PNB electrodeposited the materials, VG, DS, ALH and GR developed the electrodeposition precursors, YH and RB performed the TEM imaging. NA and YJN composed the manuscript with contributions from all authors. PNB, CHDG, ALH and GR conceived the research concept.

Notes

The authors declare no competing interest.

Acknowledgements

The research work reported in this article was financially supported by the Engineering and Physical Sciences Research Council (EPSRC) through the research grant EP/P025137/1 (2D layered transition metal dichalcogenide semiconductors via non-aqueous electrodeposition) and the programme grant

References

(1) Wang, X.-F.; Tian, H.; Liu, Y.; Shen, S.; Yan, Z.; Deng, N.; Yang, Y.; Ren, T.-L. Two-Mode MoS₂ Filament Transistor with Extremely Low Subthreshold Swing and Record High On/Off Ratio. *ACS Nano* **2019**, *13*, 2205–2212.

(2) Yin, Z.; Li, H.; Li, H.; Jiang, L.; Shi, Y.; Sun, Y.; Lu, G.; Zhang, Q.; Chen, X.; Zhang, H. Single-Layer MoS₂ Phototransistors. *ACS Nano* **2012**, *6*, 74–80.

(3) Nalwa, H. S. A Review of Molybdenum Disulfide (MoS₂) Based Photodetectors: From Ultra-Broadband, Self-Powered to Flexible Devices. *RSC Adv.* **2020**, *10*, 30529–30602.

(4) Kumar, R.; Zheng, W.; Liu, X.; Zhang, J.; Kumar, M. MoS₂-Based Nanomaterials for Room-Temperature Gas Sensors. *Adv. Mater. Technol.* **2020**, *5*, 1901062.

(5) Bertolazzi, S.; Brivio, J.; Kis, A. Stretching and Breaking of Ultrathin MoS₂. *ACS Nano* **2011**, *5*, 9703–9709.

(6) Li, N.; Wang, Q.; Shen, C.; Wei, Z.; Yu, H.; Zhao, J.; Lu, X.; Wang, G.; He, C.; Xie, L.; Zhu, J.; Du, L.; Yang, R.; Shi, D.; Zhang, G. Large-Scale Flexible and Transparent Electronics Based on Monolayer Molybdenum Disulfide Field-Effect Transistors. *Nat. Electron.* **2020**, *3*, 711–717.

(7) Noori, Y. J.; Thomas, S.; Ramadan, S.; Smith, D. E.; Greenacre, V. K.; Abdelazim, N.; Han, Y.; Beanland, R.; Hector, A. L.; Klein, N.; Reid, G.; Bartlett, P. N.; Kees de Groot, C. H. Large-Area Electrodeposition of Few-Layer MoS₂ on Graphene for 2D Material Heterostructures. *ACS Appl. Mater. Interfaces* **2020**, *12*, 49786–49794.

(8) Thomas, S.; Smith, D. E.; Greenacre, V. K.; Noori, Y. J.; Hector, A. L.; Groot, C. H. (Kees) de; Reid, G.; Bartlett, P. N. Electrodeposition of MoS₂ from Dichloromethane. *J. Electrochem. Soc.* **2020**, *167*, 106511.

(9) Zhang, W.; Huang, J.-K.; Chen, C.-H.; Chang, Y.-H.; Cheng, Y.-J.; Li, L.-J. High-Gain Phototransistors Based on a CVD MoS₂ Monolayer. *Adv. Mater.* **2013**, *25*, 3456–3461.

(10) Chen, J.; Tang, W.; Tian, B.; Liu, B.; Zhao, X.; Liu, Y.; Ren, T.; Liu, W.; Geng, D.; Jeong, H. Y.; Shin, H. S.; Zhou, W.; Loh, K. P. Chemical Vapor Deposition of High-Quality Large-Sized MoS₂ Crystals on Silicon Dioxide Substrates. *Adv. Sci.* **2016**, *3*, 1500033.

(11) Tao, J.; Chai, J.; Lu, X.; Wong, L. M.; Wong, T. I.; Pan, J.; Xiong, Q.; Chi, D.; Wang, S. Growth of Wafer-Scale MoS₂ Monolayer by Magnetron Sputtering. *Nanoscale* **2015**, *7*, 2497–2503.

(12) Tang, X.; Reckinger, N.; Poncelet, O.; Louette, P.; Ureña, F.; Idrissi, H.; Turner, S.; Cabosart, D.; Colomer, J.-F.; Raskin, J.-P.; Hackens, B.; Francis, L. A. Damage Evaluation in Graphene Underlying Atomic Layer Deposition Dielectrics. *Sci. Rep.* **2015**, *5*, 13523.

(13) Ojo, A. A.; Dharmadasa, I. M. Electroplating of Semiconductor Materials for Applications in Large Area Electronics: A Review. *Coatings* **2018**.

(14) Gerein, N. J.; Haber, J. A. Effect of Ac Electrodeposition Conditions on the Growth of High Aspect Ratio Copper Nanowires in Porous Aluminum Oxide Templates. *J. Phys. Chem. B* **2005**, *109*, 17372–17385.

(15) Wang, H.-F.; Tang, C.; Zhang, Q. A Review of Graphene-Based 3D van Der Waals Hybrids and Their Energy Applications. *Nano Today* **2019**, *25*, 27–37.

(16) Huang, R.; Kissling, G. P.; Kashtiban, R.; Noori, Y. J.; Cicvarić, K.; Zhang, W.; Hector, A. L.; Beanland, R.; Smith, D. C.; Reid, G.; Bartlett, P. N.; de Groot, C. H. (Kees). Towards a 3D GeSbTe Phase Change Memory with Integrated Selector by Non-Aqueous Electrodeposition. *Faraday Discuss.* **2019**, *213*, 339–355.

(17) Bartlett, P. N.; Benjamin, S. L.; (Kees) de Groot, C. H.; Hector, A. L.; Huang, R.; Jolley, A.; Kissling, G. P.; Levason, W.; Pearce, S. J.; Reid, G.; Wang, Y. Non-Aqueous Electrodeposition of Functional Semiconducting Metal Chalcogenides: Ge₂Sb₂Te₅ Phase Change Memory. *Mater. Horizons* **2015**, *2*, 420–426.

(18) Jeon, J.; Jang, S. K.; Jeon, S. M.; Yoo, G.; Jang, Y. H.; Park, J.-H.; Lee, S. Layer-Controlled CVD Growth of Large-Area Two-Dimensional MoS₂ Films. *Nanoscale* **2015**, *7*, 1688–1695.

(19) Hudson, J. L.; Tsotsis, T. T. Electrochemical Reaction Dynamics: A Review. *Chem. Eng. Sci.* **1994**, *49*, 1493–1572.

(20) Andricacos, P. C.; Uzoh, C.; Dukovic, J. O.; Horkans, J.; Deligianni, H. Damascene Copper Electroplating for Chip Interconnections. *IBM J. Res. Dev.* **1998**, *42*, 567–574.

(21) Sharma, A.; Mahlouji, R.; Wu, L.; Verheijen, M. A.; Vandalon, V.; Balasubramanyam, S.; Hofmann, J. P.; (Erwin) Kessels, W. M. M.; Bol, A. A. Large Area, Patterned Growth of 2D MoS₂ and Lateral MoS₂–WS₂ Heterostructures for Nano- and Opto-Electronic Applications. *Nanotechnology* **2020**, *31*, 255603.

(22) Chhowalla, M.; Jena, D.; Zhang, H. Two-Dimensional Semiconductors for Transistors. *Nat. Rev. Mater.* **2016**, *1*, 16052.

(23) Giannazzo, F.; Greco, G.; Roccaforte, F.; Sonde, S. S. Vertical Transistors Based on 2D Materials: Status and Prospects. *Crystals* **2018**, *8*, 70.

(24) Liu, Y.; Weiss, N. O.; Duan, X.; Cheng, H.-C.; Huang, Y.; Duan, X. Van Der Waals Heterostructures and Devices. *Nat. Rev. Mater.* **2016**, *1*, 16042.

(25) Zach, M. P.; Ng, K. H.; Penner, R. M. Molybdenum Nanowires by Electrodeposition. *Science (80-.)* **2000**, *290*, 2120 LP – 2123.

(26) Menke, E. J.; Thompson, M. A.; Xiang, C.; Yang, L. C.; Penner, R. M. Lithographically Patterned Nanowire Electrodeposition. *Nat. Mater.* **2006**, *5*, 914–919.

(27) Xiang, C.; Kung, S.-C.; Taggart, D. K.; Yang, F.;

Thompson, M. A.; Güell, A. G.; Yang, Y.; Penner, R. M. Lithographically Patterned Nanowire Electrodeposition: A Method for Patterning Electrically Continuous Metal Nanowires on Dielectrics. *ACS Nano* **2008**, *2*, 1939–1949.

(28) Walter, E. C.; Zach, M. P.; Favier, F.; Murray, B. J.; Inazu, K.; Hemminger, J. C.; Penner, R. M. Metal Nanowire Arrays by Electrodeposition. *ChemPhysChem* **2003**, *4*, 131–138.

(29) de Leeuw, D. M.; Kraakman, P. A.; Bongaerts, P. F. G.; Mutsaers, C. M. J.; Klaassen, D. B. M. Electroplating of Conductive Polymers for the Metallization of Insulators. *Synth. Met.* **1994**, *66*, 263–273.

(30) Kobayashi, C.; Saito, M.; Homma, T. Laterally Enhanced Growth of Electrodeposited Au to Form Ultrathin Films on Nonconductive Surfaces. *Electrochim. Acta* **2012**, *74*, 235–243.

(31) Albu-Yaron, A. A Study on MoS₂ Thin Films Electrochemically Deposited in Ethylene Glycol at 165°C. *Electrochem. Solid-State Lett.* **1999**, *2*, 627.

(32) Chaabani, R.; Lamouchi, A.; Mari, B.; Chtourou, R. Effect of Sulfurization on Physical and Electrical Properties of MoS₂ Films Synthesized by Electrodeposition Route. *Mater. Res. Express* **2019**, *6*, 115902.

(33) Lamouchi, A.; Assaker, I. Ben; Chtourou, R. Effect of Annealing Temperature on the Structural, Optical, and Electrical Properties of MoS₂ Electrodeposited onto Stainless Steel Mesh. *J. Mater. Sci.* **2017**, *52*, 4635–4646.

(34) Xiao, J.; Long, M.; Li, X.; Zhang, Q.; Xu, H.; Chan, K. S. Effects of van Der Waals Interaction and Electric Field on the Electronic Structure of Bilayer MoS₂. *J. Phys. Condens. Matter* **2014**, *26*, 405302.

(35) Eda, G.; Yamaguchi, H.; Voiry, D.; Fujita, T.; Chen, M.; Chhowalla, M. Photoluminescence from Chemically Exfoliated MoS₂. *Nano Lett.* **2011**, *11*, 5111–5116.

(36) Wu, G.; Wang, X.; Chen, Y.; Wang, Z.; Shen, H.; Lin, T.; Hu, W.; Wang, J.; Zhang, S.; Meng, X.; Chu, J. Ultrahigh Photoresponsivity MoS₂ Photodetector with Tunable Photocurrent Generation Mechanism. *Nanotechnology* **2018**, *29*, 485204.

(37) Perea-López, N.; Lin, Z.; Pradhan, N. R.; Iñiguez-Rábago, A.; Laura Elías, A.; McCreary, A.; Lou, J.; Ajayan, P. M.; Terrones, H.; Balicas, L.; Terrones, M. CVD-Grown Monolayered MoS₂ as an Effective Photosensor Operating at Low-Voltage. *2D Mater.* **2014**, *1*, 11004.

(38) Duan, X.; Wang, C.; Shaw, J. C.; Cheng, R.; Chen, Y.; Li, H.; Wu, X.; Tang, Y.; Zhang, Q.; Pan, A.; Jiang, J.; Yu, R.; Huang, Y.; Duan, X. Lateral Epitaxial Growth of Two-Dimensional Layered Semiconductor Heterojunctions. *Nat. Nanotechnol.* **2014**, *9*, 1024–1030.

(39) Wang, J.; Li, Z.; Chen, H.; Deng, G.; Niu, X. Recent Advances in 2D Lateral Heterostructures. *Nano-Micro Lett.* **2019**, *11*, 48.